CHAPTER 6

HYBRID OM-ACE TRANSMISSION

6.1 INTRODUCTION

In this chapter, the ease with which an ACE method, which is a well-established PAPR reduction method recommended by the DVB - T2 standard [95], may be incorporated into an OM-OFDM transmission is discussed. The PAPR benefits derived from both the OM-OFDM and ACE methods are inherited by this offset modulation with the active constellation extension (OM-ACE) method. Although this chapter confines its discussion to this particular case, it demonstrates the manner in which the various other PAPR reduction methods may be incorporated into an OM-OFDM transmission. This chapter begins by introducing this hybrid OM-ACE method.

6.2 PROPOSED OM-ACE METHOD

Consider the complex output of an N-point inverse fast Fourier transformed OFDM signal, given by

$$m_n = \frac{1}{\sqrt{N}} \sum_{k=0}^{N-1} X_k e^{j\frac{2\pi nk}{N}}, \qquad n = 0, 1, ..., N-1. \tag{6.1}$$

In Eq (6.1), X_k represents the complex signal output $(a_k + jb_k)$ of the IFFT. This signal may be modulated using the method which follows.

$$\Phi_{1n} = \frac{\Re(m(t))}{\varsigma} \quad \text{and} \quad \Phi_{2n} = \frac{\Im(m(t))}{\varsigma} \tag{6.2}$$

In Eq (6.2), $\Re$ and $\Im$, refer to the real and imaginary parts of the OFDM message signal and ς refers to a constant division term. These Φ_{1n} and Φ_{2n} terms are passed through a DAC and may now be combined into a unique co-sinusoid

$$\cos(2\pi f_c t + \Phi_1(t) + \Psi_{os}) - \cos(2\pi f_c t + \Phi_2(t)) \tag{6.3}$$

where, $\Phi_1(t)$ and $\Phi_2(t)$ represent the equivalent real and imaginary OFDM phase mapping. When $\Phi_1(t) + \Psi_{os} \leq \pi/2$, this allows the original $\Phi_1(t)$ expression to be accurately extracted at the receiver. In order to maintain this limit, the ACE method can be used. A block

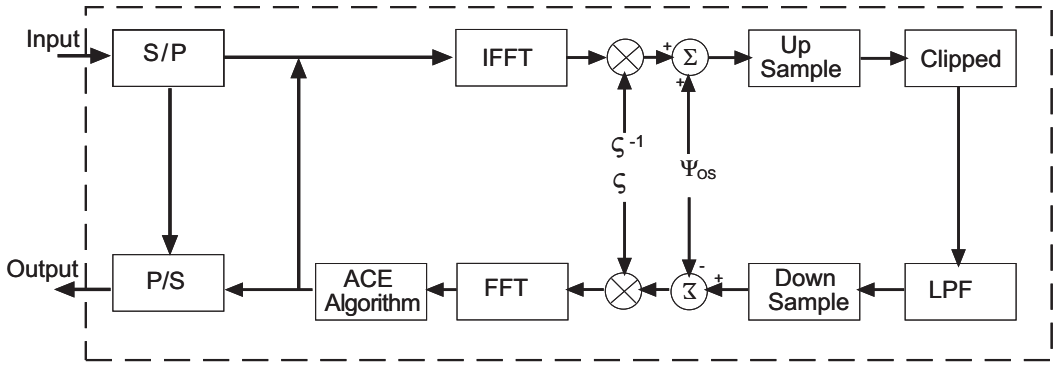

Figure 6.1: ACE structure

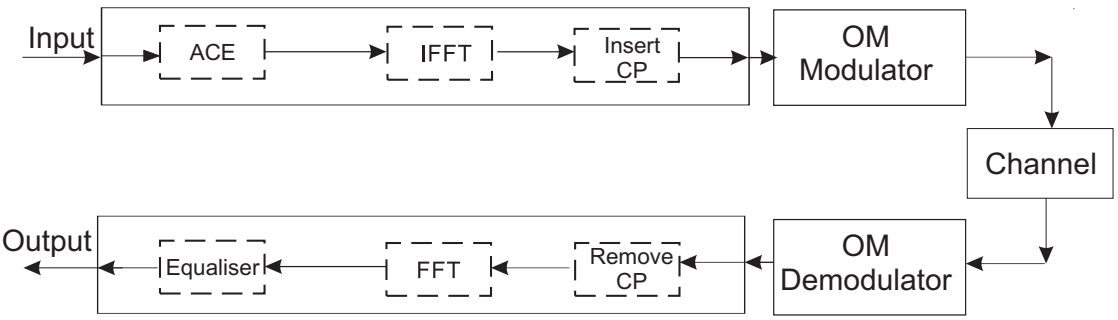

Figure 6.2: OM-ACE transmitter receiver structure

diagram, depicted in Fig. 6.1 and Fig. 6.2, shows the processes involved during an OM-ACE transmission. The incoming constellation is intelligently extended by using the ACE method (Fig. 6.1) such that $\Phi_1(t) + \Psi_{os} \leq \pi/2$. The message signal is inverse fast Fourier transformed and a cyclic prefix is amended to the OFDM signal. Thereafter, the signal is modulated using an OM modulator (Fig. 3.2), after which the signal is passed through a channel. The subsequent incoming signal is passed through an OM demodulator (Fig. 3.3) to recover the OFDM signal. The cyclic prefix is removed and a FFT is performed. Thereafter, equalisation is performed to mitigate the channel effects. The equalisation process is identical to that used for an OFDM transmission; CSI is extracted from the pilot symbols and used during the equalisation process to mitigate the channel effects.

6.3 BIT ERROR RATE CHARACTERISTICS OF AN OM-ACE TRANSMISSION

In this section the reasoning for the inclusion of the ACE method in an OM-OFDM transmission will be addressed. Based on work from Chapter 3 (Eq (3.91)), suppose the QAM theoretical BER for an OM-ACE transmission through an AWGN channel can be written as

$$BER_{QAM} \approx \frac{k \cdot \ell(M-2) + \wp \cdot k(M - 2\sqrt{M} + 2)}{M \cdot k^2} + \frac{\wp \cdot \ell(2\sqrt{M} - M - 1)}{M \cdot k^2} \tag{6.4}$$

where

$$\wp = \operatorname{erfc}\left(\sqrt{\frac{k\xi_b}{\xi_{av}N_o}}\right) \quad \text{and} \quad \ell = \operatorname{erfc}\left(\sqrt{\frac{4k\sin^2(-\frac{\varphi}{2})\xi_b}{\xi_{av}N_o}}\right). \tag{6.5}$$

As previously mentioned in Section 6.2, $\Phi_1(t) + \Psi_{os} \leq \pi/2$, this allows the original $\Phi_1(t)$ expression (adapted real phase deviation) to be accurately extracted at the receiver. The ACE method, or any alternate method discussed in Section 2.8, may be used to reduce the adapted real phase deviations. A traditional ACE transmission makes use of an iterative process, which is used to find an optimum real and imaginary constellation extension. When using the ACE method in an OM-ACE transmission and limiting its application to only the

adapted real phase deviations, the iterative nature of the process is reduced when compared to a traditional ACE transmission, which involves extending both the real and imaginary constellation. The inclusion of the ACE method in an OM-OFDM method should allow both the Ψ_{os} and γ term to approach the optimum operating point closely. This would improve the BER characteristics of an OM-ACE transmission.

With these guidelines, the theoretically presented BER expression for an OM-ACE transmission needed to be validated. By means of a simulation (the 2k mode of the DVB - T2 standard [95]), 16-QAM Gray-coded OM-OFDM and OM-ACE data were transmitted through an AWGN channel. The parameters used for the 16-QAM OM-OFDM and OM-ACE transmission are given in Table 6.1 and Table 6.2, respectively. In both Table 6.1 and Table 6.2 the φ term is calculated, as indicated in Table 3.2, by substituting α, ς, Ψ_{os} and γ terms into the φ expression. The specific terms (ς and Ψ_{os}) are chosen to minimise the BER degradation and the α ($\alpha \approx \alpha_1 \approx \alpha_2$) term is obtained as indicated in Eq (3.18) and Eq (3.19).

Table 6.1: Parameters for a 16-QAM OM-OFDM system ($\alpha = 0.07408$))

PAPR	Ψ_{os}	ς	γ	φ
8 dB	1.5	10000/4096	0.973	0.3
9 dB	1.5	10000/4096	0.98	0.4
10 dB	1.5	10000/4096	0.985	0.5
11 dB	1.5	10000/4096	0.988	0.6
12 dB	1.5	10000/4096	1	1.0

Table 6.2: Parameters for a 16-QAM OM-ACE system ($\alpha = 0.07408$)

PAPR	Ψ_{os}	ς	γ	φ
8 dB	1.55	10000/4096	0.975	0.3
9 dB	1.55	10000/4096	0.982	0.4
10 dB	1.55	10000/4096	0.988	0.5
11 dB	1.55	10000/4096	0.9919	0.7
11.4 dB	1.55	10000/4096	1	1.0

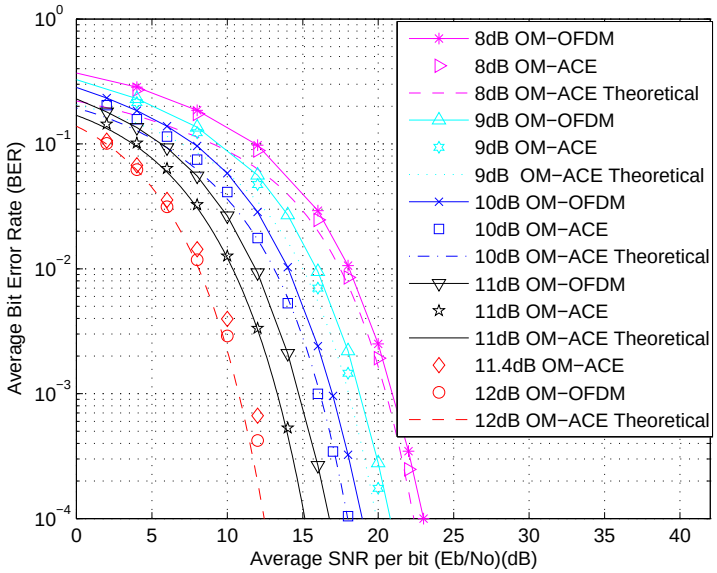

Figure 6.3: A BER comparison between an OM-ACE, theoretically predicted OM-ACE (Eq (6.4)) and OM-OFDM transmission in an AWGN channel.

From the BER comparison depicted in Fig. 6.3, it can be seen that the theoretically predicted OM-ACE results and the simulated OM-ACE results correlate reasonably well, thus validating the theoretical expression. Furthermore, a comparison between Table 6.1 and Table 6.2 indicates that the Ψ_{os} term has increased. This is possible because of the introduction of the ACE method. The γ term has also increased and the combination of an increase in the Ψ_{os} and γ term should result in an improvement in the OM-ACE BER characteristics, when compared to an OM-OFDM transmission (without ACE). This observation is corroborated, as depicted in Fig. 6.3, by the results presented.

6.4 RESULTS AND DISCUSSION

In this section, a 16-QAM Gray-coded 2k mode of the DVB-T2 [95] standard was used to compare OFDM, OM-OFDM, ACE, OM-ACE and a classically clipped OFDM transmission. When classically clipping a signal to limit the out-of-band distortion, the clipped OFDM signal was filtered before transmission with an 9^{th} order Butterworth low-pass filter.

The ACE method made use of the POCS [69, 73] approach, which involved clipping the signal with a 7 dB clipping threshold and thereafter using a 4^{th} order Butterworth low-pass filter. This iterative POCS approach was terminated after 30 iterations, since this proved to be a convergence point. After an exhaustive search, all the clipping thresholds and filter parameters used in this section were found to be optimal solutions.

In all the BER results which follow, a 16-QAM Gray-coded 2k mode of the DVB-T2 standard was used to transmit OM-ACE, OM-OFDM, OFDM and clipped OFDM data through a 5-tap typical-urban frequency selective fading channel. For the OM-ACE, OM-OFDM, OFDM and clipped OFDM transmissions, CSI is extracted from the pilot symbols and used during the equalisation process to mitigate the effects of fading. The pilot symbol placement can be found in the DVB-T2 standard. Similarly, the 5-tap typical-urban area model was obtained from Patzold [96]. Identical throughputs were used to ensure a fair comparison between the various methods and perfect carrier and timing synchronisation is assumed. All the methods conform to both the spectrum mask and throughput requirements imposed by the DVB-T2 standard. The parameters used for the OM-OFDM and OM-ACE transmission are given in Table 6.1 and Table 6.2 respectively.

6.4.1 Bit error rate performance analysis

OFDM, clipped OFDM, OM-OFDM and OM-ACE data were sent through a 5-tap typical-urban area by using the parameters previously mentioned. The average PAPR of an OFDM transmission when using the 2k mode of the DVB-T2 standard, according to simulations, is 12 dB. This PAPR is fixed for an OFDM transmission and as discussed in Section 2.8, may only be changed by adopting one or some of the PAPR reduction methods. For the ACE and OM-ACE method, the initial averaged PAPRs are 11.83 and 11.37 respectively; these are from henceforth referred to as an ACE and an OM-ACE transmission.

Unlike the OFDM and ACE transmission, both the OM-OFDM and OM-ACE methods allow the PAPR of the signal to be varied, while maintaining identical throughput

and bandwidth occupancy as an OFDM and ACE transmission. A direct comparison, as

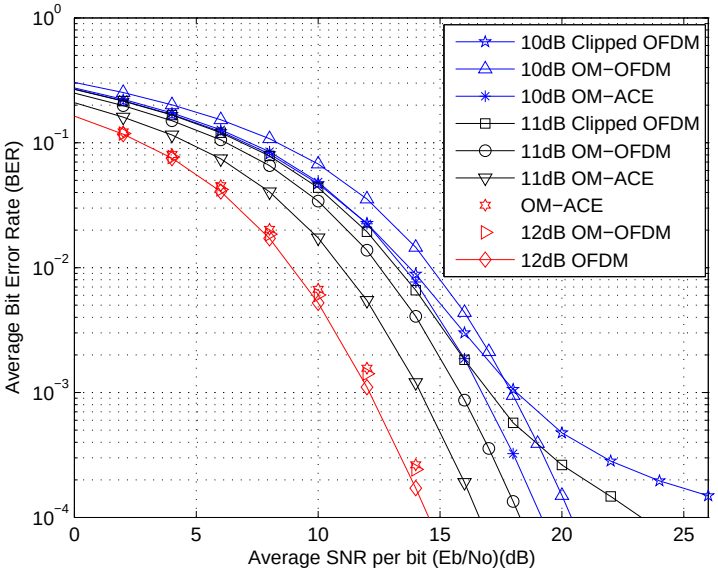

Figure 6.4: BER comparisons for a 16-QAM transmission through a 5-tap typical-urban area.

shown in Fig. 6.4, between an OFDM, OM-OFDM and OM-ACE transmission shows that all three methods offered similar BER characteristics. However, a comparison between an OM-ACE (PAPR 11.37 dB), OFDM (PAPR 12 dB) and OM-OFDM (PAPR 12 dB) transmission, indicates that the OM-ACE (PAPR 11.37 dB) transmission offers on average a 0.63 dB PAPR reduction for similar BER characteristics. Another comparison, depicted in Fig. 6.4, between OM-ACE and a clipped OFDM transmission shows that the clipped OFDM transmission reaches a BER plateau (PAPR $\leq$ 10 dB), whereas the OM-ACE does not result in this BER effect in this case. The BER performance of the ACE methods is not presented, since it resembles that of an OM-ACE and OFDM transmission.

6.4.2 Power performance decision metric performance analysis

A direct comparison between OM-ACE, OM-OFDM, ACE, OFDM and clipped OFDM transmissions is facilitated by utilising the power performance decision metric discussed in Section 3.7. The results from such an implementation, depicted in Fig. 6.5, used a standard OTS AN10858 [98] RF power amplifier. From this comparison it should be noted that the

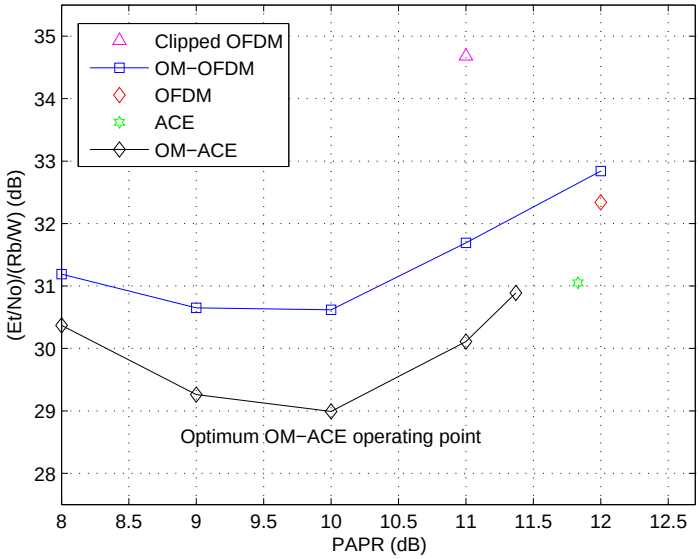

Figure 6.5: System performance for a 16-QAM constellation at a BER of 10^{-4} for a AN10858 RF power amplifier.

clipped OFDM results have been abridged because the clipped OFDM BER plateaued, thus it was unable to produce the specific BER. When using this standard OTS power amplifier, the optimum operating point for an OM-ACE and OM-OFDM transmission is at a PAPR of 10 dB, where a minimum decision metric occurs. For the ACE and clipped OFDM transmission the optimum operating points are 11.83 dB and 11 dB respectively.

At these optimum operating points, the OM-ACE transmission is shown to offer a net power performance gain of 1.6 dB (31.62%), 2 dB (37.71%), 3 dB (50.83%) and 5.7 dB (73.02%), at a BER of 10^{-4}, when compared to OM-OFDM, ACE, OFDM and clipped OFDM transmissions, respectively. The decision metric also suggests that the OM-ACE method's average PAPR value may be lowered to 8 dB (thus a 4 dB average PAPR reduction when compared to the original OFDM transmission), while maintaining a performance improvement over OM-OFDM, ACE, OFDM and clipped OFDM transmissions.

This power performance decision metric result might appear to be misleading, since at a BER of 10^{-4}, as shown in Fig. 6.4, this 3 dB net gain is not expected. The 3 dB net power performance gain is attributed to the fact that the PAE curve of a typical amplifier

is exponentially shaped [98], instead of being linear. Hence, the exponential relationship between PAPR (dB) and PAE, instead of a linear relationship, results in this exponential increase in efficiency.

6.4.3 Complementary cumulative distribution function performance analysis

Using the optimum operating points obtained from the power performance decision metric in the previous sub-section, the complementary cumulative distribution function, depicted in Fig. 6.6, was used to compare the PAPR characteristics of clipped OFDM, OFDM, ACE and OM-ACE transmissions. At the optimum operating points, the OM-ACE transmission

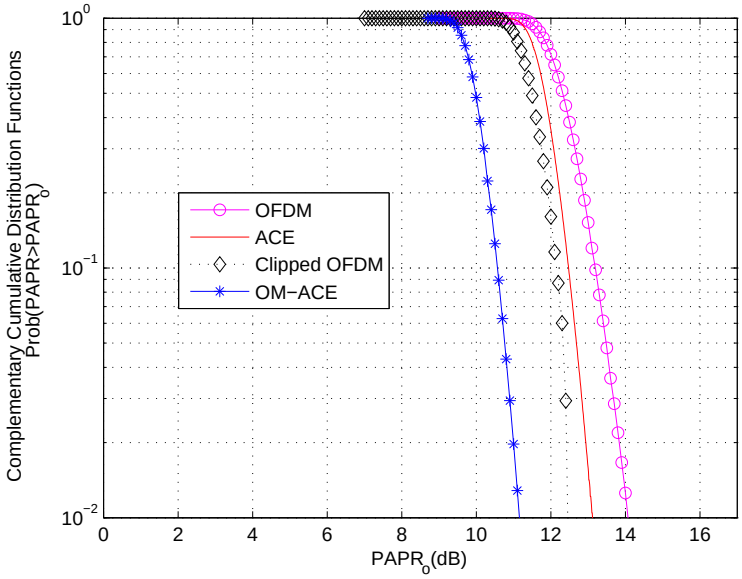

Figure 6.6: Complementary cumulative distribution functions for a 16-QAM constellation.

is shown to offer a PAPR reduction of 2.6 dB, 1.9 dB and 1.6 dB (at a CCDF of 10^{-1}) when compared to OFDM, ACE and clipped OFDM transmissions respectively. Although the clipping method offers attractive CCDF results, the subsequent BER characteristics are not attractive.

6.5 CONCLUSIONS

In this chapter, an OM-ACE method has been proposed to control the PAPR of an OFDM DVB-T2 transmission, for a targeted BER. A closed-form theoretical BER expression for this OM-ACE transmission is presented. This mathematical BER expression has been shown to agree with the simulated results, thus further validating the derivation.

Thereafter, when utilising the power performance decision metric, the OM-ACE transmission is shown to offer a net power performance gain of between 5.7 dB-1.6 dB (73.02%-31.62%), at a BER of 10^{-4}, when compared to clipped OFDM, OFDM, OM-OFDM and ACE transmissions, in a frequency selective fading channel. By using a CCDF, the OM-ACE method is shown to offer a PAPR reduction of between 2.6 dB - 1.6 dB (at a CCDF of 10^{-1}) when compared to OFDM, ACE and clipped OFDM transmissions.

CHAPTER 7

A COGNITIVE RADIO APPLICATION OF OM-OFDM

7.1 INTRODUCTION

In November 2002, the federal communications commission (FCC) published a report, which contained results obtained from limited spectrum measurements in urban areas [102]. This report suggested that there was some evidence indicating that the shortage of spectrum is often a spectrum access problem. That is, the spectrum resource is available, but its use is compartmented by traditional policies based on traditional technologies. In August 2005 [103], during spectrum occupancy measurements at six locations, it was shown that the average occupancy over all of the locations was 5.2%. As the demand for bandwidth increases, the natural approach would be the better utilisation of such bandwidth by spectrum sharing. It is these factors which have made cognitive radio (CR) a promising concept. In this chapter [104] the detection characteristics of OM-OFDM and OFDM transmissions are investigated for cognitive radio applications.

7.2 COGNITIVE RADIO

The word cognitive radio was proposed by Mitola [105] [106], although the cognitive concept was already previously known [107]. Thereafter, the Defence Advanced Research Project Agency (DARPA) was the first to launch an initiative employing CR called neXt

Generation communication systems, aimed at developing technologies to dynamically manage the spectrum [108]. The cognitive concept currently involves thinking of frequency spectrum in terms of spectrum holes. A spectrum hole is a band of frequencies assigned to a primary user (the owner of the spectrum), but at a particular time and geographic location not being occupied by this user. A secondary user is allowed to access this spectrum hole, and later vacate it, provided that it does not interfere with the primary user. This process exploits spectrum holes and ultimately leads to efficient bandwidth utilisation. While the cognitive radio concept is still in its conceptual stage, the benefits of spectrum sharing with interference avoidance has already been demonstrated by the co-existence between the IEEE 802.11 (Wi-Fi) and IEEE 802.15 (bluetooth) networks. Regulators are willing to go further by experimenting with spectrum sharing of the TV band in the development of the IEEE 802.22 standard. A technical proof and feasibility of this concept would further clear the way for regulatory approval for spectrum-sharing licensing.

Thus far the secondary user is seen as an opportunistic user, which continuously senses different spectrums and when it identifies a spectrum hole, accesses it. The secondary user later vacates the spectrum, such that it does not interfere with the primary user. Various sensing methods such as matched filtering, energy detection and cyclostationary feature detection [109, 110], amongst others, have been recommended. Of the three methods mentioned, energy detection requires the lowest complexity and requires no prior information about the signal.

In this chapter, the energy detection method will be used to detect a DVB-T2 [95] OFDM transmission. This type of energy detection would typically be employed by a secondary user in the spectrum sensing of a TV band in the development of the IEEE 802.22 standard. The problem associated with such an OFDM transmission is its high PAPR. As previously stated, OM-OFDM has been proposed to control the PAPR of an OFDM transmission. This OM-OFDM method has been shown to offer a significant power performance improvement when compared to a traditional OFDM transmission. In this chapter, the ability of a secondary user to detect OM-OFDM and OFDM transmissions will be investigated.

7.3 BANDWIDTH OCCUPANCY OF OFFSET MODULATION

In this section the bandwidth occupancy of an OM-OFDM transmission will be investigated to highlight its attractive detection characteristics. As previously described (Eq (3.15)), the bandwidth occupancy of an OM-OFDM transmission can be written as

$$u_n = \sum_{y=0}^{2x} \left| \sum_{z=0}^{2x-y} 2\sin\left(\frac{\pi(2x-2z-y)\pm 2\Psi_{os}}{4}\right) \cdot J_{|-x+z|}(\beta_1) \left(\frac{|-x+z+\frac{1}{2}|}{-x+z+\frac{1}{2}}\right)^{|-x+z|} \cdot J_{|x-y-z|}(\beta_2) \left(\frac{|x-y-z+\frac{1}{2}|}{x-y-z+\frac{1}{2}}\right)^{|x-y-z|} \cdot \sin\left(2\pi(f_c+yf_d)+\frac{2\Psi_{os}\pm y\pi}{4}\right) \right|. \quad (7.1)$$

Then by inspection of Eq (7.1) for this particular case, as depicted in Fig. 7.1, the frequency spectrum and its corresponding amplitude components are shown. The dominant frequency

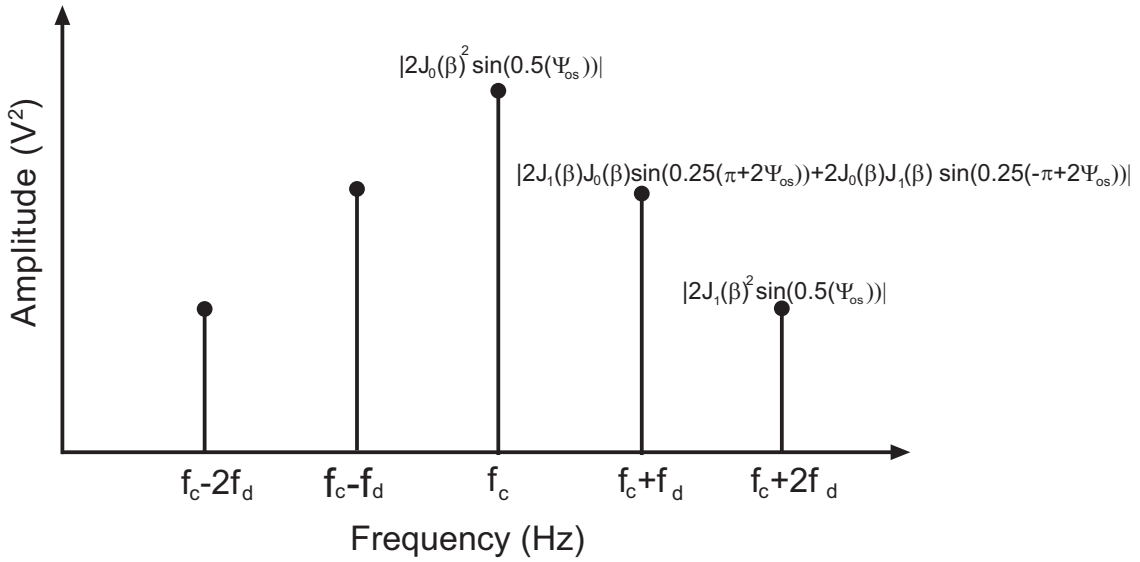

Figure 7.1: Theoretically derived (Eq (7.1)) frequency spectrum of an OM-OFDM signal.

component is given by $2J_0(\beta)^2\sin(2\pi f_c t - \frac{\Psi_{os}}{2})$, provided $\Psi_{os} >> \Phi_2(t) - \Phi_1(t)$. It is the prominence of this dominant frequency component that should significantly aid in the detection of an OM-OFDM transmission by a secondary user, when using energy detection.

7.4 RECEIVER OPERATING CHARACTERISTIC DERIVATION

During energy detection as described in [111] (depicted in Fig. 7.2), the received signal is first pre-filtered by a band-pass filter. The output of this filter is then squared and integrated to produce a measure of the energy of the received waveform. The subsequent output of the

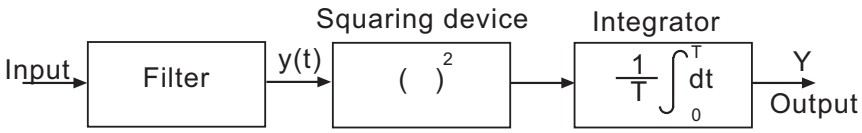

Figure 7.2: Energy detection [111]

integrator, denoted by Y, will act as a detection test for the

$$\begin{aligned} H_0, &\quad \text{the input is noise alone and} \\ H_1, &\quad \text{the input is a signal plus noise} \end{aligned} \tag{7.2}$$

hypothesis. The probability of a detection (P_d) and the probability of a false alarm can be determined by

$$P_d = P(Y > \lambda | H_1) \tag{7.3}$$

$$P_{fa} = P(Y > \lambda | H_o) \tag{7.4}$$

where λ is the decision threshold, Y has a chi-square distribution for both the H_0 (central chi-square distribution) and H_1 (non-central chi-square distribution) cases. The subsequent probability density function (PDF) of Y [3, Eq (2.1-110) and Eq (2.1-118)], when $y \geq 0$ can be written as

$$f_Y(y) = \begin{cases} \frac{y^{u-1} e^{\frac{-y}{2\sigma^2}}}{\sigma^{2u} 2^u \Gamma(u)} \\ \frac{1}{2\sigma^2} \left(\frac{y}{a \cdot \Upsilon^2} \right)^{\frac{u-1}{2}} e^{-\frac{a \cdot \Upsilon^2 + y}{2\sigma^2}} J_{u-1} \left(\frac{\sqrt{y \cdot a \cdot \Upsilon^2}}{\sigma^2} \right) \end{cases} \tag{7.5}$$

where u refers to an even number of degrees of freedom, σ^2 is the variance, $\Gamma(.)$ is the gamma function, Υ is the signal-to-noise ratio $\left(\Upsilon = \frac{E_s}{N_0} \right.$, where E_s is the signal energy and N_0 is the

one-sided power spectral density$\Big)$ and a is the non-centrality parameter of the distribution. After using [3, Eq (2.1-124)], the P_d can be shown to be written as

$$P_d = Q_u\left(\frac{\sqrt{a\cdot\Upsilon^2}}{\sigma},\frac{\sqrt{\lambda}}{\sigma}\right) \tag{7.6}$$

in Eq (7.6), $Q_u(.,.)$ is the Marcum Q-function [3]. From Eq (7.5), it can be shown that

$$P_{fa} = \int_{\frac{\lambda}{2\sigma^2}}^{\infty}\frac{e^{-t}t^{u-1}}{\Gamma(u)}dt. \tag{7.7}$$

Consider the upper incomplete gamma function $\Gamma(.,.)$, and the lower incomplete gamma function $\chi(.,.)$, defined as [91, Eq (6.5.3), Eq (6.5.2)]

$$\Gamma(u,x) = \Gamma(u)-\chi(u,x) = \int_x^{\infty}e^{-t}t^{u-1}dt \quad \text{and} \tag{7.8}$$

$$\chi(u,x) = \int_0^{x}e^{-t}t^{u-1}dt. \tag{7.9}$$

Using Eq (7.8) to evaluate Eq (7.7), results in

$$P_{fa} = \frac{\Gamma(u,\frac{\lambda}{2\sigma^2})}{\Gamma(u)} = \frac{\Gamma(u)-\chi(u,\frac{\lambda}{2\sigma^2})}{\Gamma(u)}. \tag{7.10}$$

If the received signal strength follows a Rician distribution, the PDF ($\Upsilon \geq 0$) can be written as

$$f(\Upsilon) = \frac{2\Upsilon(K+1)}{\overline{\Upsilon}}J_0\Big(2\sqrt{\frac{K(K+1)}{\overline{\Upsilon}}}\Upsilon\Big)e^{-K-\frac{(K+1)\Upsilon^2}{\overline{\Upsilon}}}. \tag{7.11}$$

In Eq (7.11), K is the Rician distribution factor and $\overline{\Upsilon}$ is the average signal-to-noise ratio. This equation (Eq (7.11)) is slightly different from that introduced by Digham et al. [112, Eq (24)] since the errors made in [112] have been corrected. The expression for the average $\overline{P_d}$ in a Rician environment is calculated by averaging the expression for P_d in AWGN (Eq (7.6)) over the Rician fading PDF (Eq (7.11)), this results in

$$F(\Upsilon) = \frac{2(K+1)}{\overline{\Upsilon}}\int_0^{\infty}\Upsilon\cdot Q_u\left(\frac{\sqrt{a\cdot\Upsilon^2}}{\sigma},\frac{\sqrt{\lambda}}{\sigma}\right)\cdot e^{\left(-K-\frac{(K+1)\Upsilon^2}{\overline{\Upsilon}}\right)}\cdot J_0\left(2\sqrt{\frac{K(K+1)}{\overline{\Upsilon}}}\Upsilon\right)d\Upsilon. \tag{7.12}$$

After using [113, Eq (45)], Eq (7.12) simplifies into

$$\overline{P_{d_{Ric}}} = Q\left(\sqrt{\frac{2aK\overline{\Upsilon}}{2\sigma^2(K+1)+a\overline{\Upsilon}}}, \sqrt{\frac{2\lambda(K+1)}{2\sigma^2(K+1)+a\overline{\Upsilon}}}\right). \tag{7.13}$$

An equation relating the P_{md} to P_{fa} for a Rician fading channel can be obtained by solving for λ in Eq (7.10). When $u = 1$, and Eq (7.8), Eq (7.9) and Eq (7.10) are used, this results in

$$P_{fa} = 1 - \frac{\chi\left(1, \frac{\lambda}{2\sigma^2}\right)}{\int_0^\infty e^{-t}dt} = 1 - \int_0^{\frac{\lambda}{2\sigma^2}} e^{-t}dt = e^{-\frac{\lambda}{2\sigma^2}}. \tag{7.14}$$

From Eq (7.14) it can be shown that $\lambda = -2\sigma^2\ln(P_{fa})$; substituting this into Eq (7.13) results in

$$\overline{P_{md\,Ric}}|_{u=1} = 1 - Q\left(\sqrt{\frac{2aK\overline{\Upsilon}}{2\sigma^2(K+1)+a\overline{\Upsilon}}}, \sqrt{\frac{-4\sigma^2(K+1)\ln P_{fa}}{2\sigma^2(K+1)+a\overline{\Upsilon}}}\right). \tag{7.15}$$

When $K = 0$, the above expression reduces to the average $\overline{P_d}$ for a Rayleigh fading channel, which can be written as

$$\begin{aligned}\overline{P_{md\,Ray}}|_{u=1} &= 1 - Q\left(0, \sqrt{\frac{-4\sigma^2\ln P_{fa}}{2\sigma^2+a\overline{\Upsilon}}}\right) \\ &= 1 - \exp\left[\frac{2\sigma^2\ln P_{fa}}{2\sigma^2+a\overline{\Upsilon}}\right].\end{aligned} \tag{7.16}$$

As previously mentioned, the σ and a term in Eq (7.15) and Eq (7.16) are signal-dependent. For an OFDM transmission it can be shown that $\sigma^2 \approx 1$ and $a \approx 2$, while similarly, for an OM-OFDM transmission

$$\sigma^2 \approx \frac{1}{\sin^2\left(\frac{-\varphi}{2}\right)} \quad \text{and} \quad a \approx 2\sqrt{2} \tag{7.17}$$

where, φ is a constant term and has been calculated as presented in Table 3.2. Previous expressions have been derived, which relate the P_{md} to P_{fa} [109, 112, 114]. However, to

Table 7.1: Parameters for a 16-QAM OM-OFDM system ($\alpha = 0.07408$)

PAPR	Ψ_{os}	ς	γ	φ
10 dB	1.5	$10000/4096$	0.985	0.505

the best of the author's knowledge, they have not been presented in such a closed-form expression, which can be used for any generic unknown deterministic signal (for instance OFDM and OM-OFDM). In order to validate the theoretical results, 16-QAM Gray-coded OFDM and OM-OFDM data were transmitted through a Rician (K=5dB) and Rayleigh fading channel by using the 2k mode of the DVB-T2 standard. In Table 7.1 the parameters used for the 16-QAM OM-OFDM transmission are given.

When using the DVB-T2 standard, OM-OFDM allows the PAPR of the signal to be varied, while maintaining identical throughput and bandwidth occupancy as an OFDM transmission. The optimum operating point for such an OM-OFDM transmission is at a 10 dB PAPR (Section 4.4). In order to offer a fair comparison, the PAPR of an OFDM transmission was reduced from 12 dB PAPR to 10 dB PAPR by using the clipping method. The ROC of a 10 dB PAPR and 12 dB PAPR clipped OFDM transmission are almost identical. When classically clipping a signal to limit the out-of-band distortion, the clipped OFDM signal was filtered before transmission with an 9^{th} order Butterworth low-pass filter. The ROC results depicted in Fig. 7.3 and Fig. 7.4 were obtained by using an energy detector. These results offer a comparison between simulated and theoretical (Eq (7.15) and Eq (7.16)) OFDM and OM-OFDM transmissions through a Rician (K=5dB) and Rayleigh fading channel, respectively.

From these comparisons, in Fig. 7.3 and Fig. 7.4, it can be seen that the theoretically predicted and simulated results correlate reasonably well, validating the derivation process. The differences between the simulated and theoretical results at high $\overline{\Upsilon}$ can be attributed to the signal being theoretically assumed to have a non-centrality chi-square distribution, for a high $\overline{\Upsilon}$ under the H_1 condition. In order to determine the assumed non-centrality chi-square distribution, various parameters (a, σ^2 and u) were used. There is a slight difference between the actual signal distribution and assumed non-centrality chi-square distribution, which

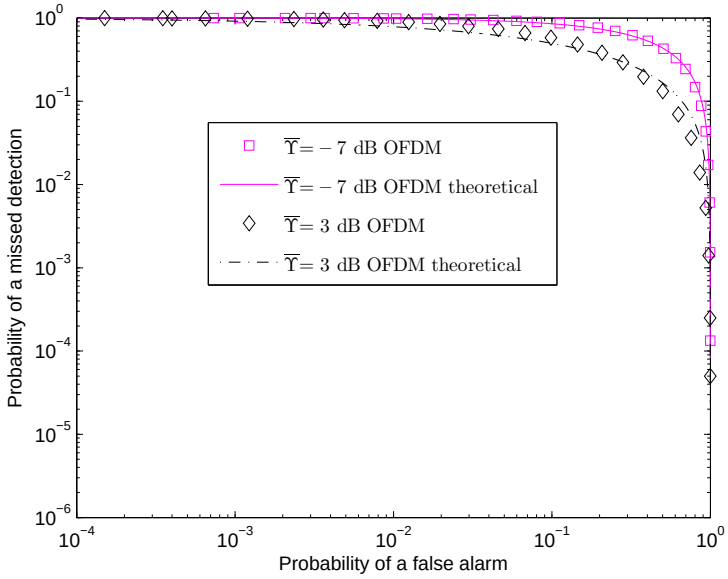

(a) A 12 dB PAPR OFDM transmission

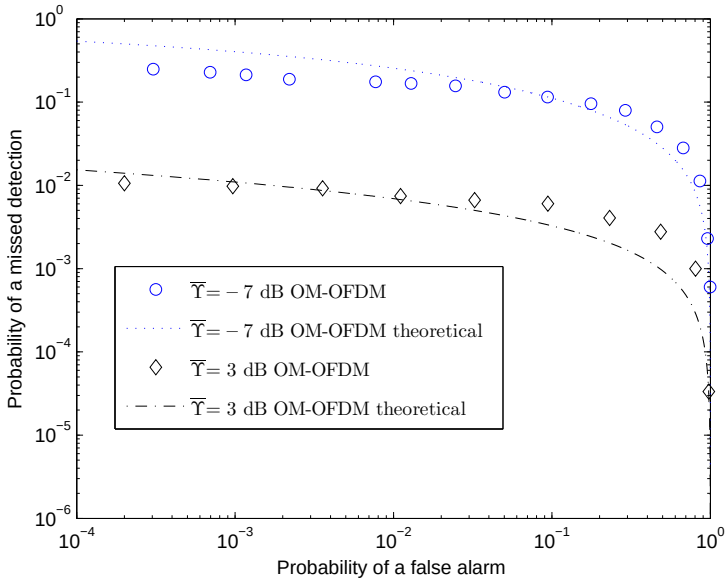

(b) OM-OFDM transmission

Figure 7.3: A ROC comparison between a theoretically predicted (Eq (7.15)) and simulated OFDM and OM-OFDM transmission through a Rician fading (K=5dB) channel.

contributes to the difference between the simulated and theoretical results. A comparison between Fig. 7.3(a) and Fig. 7.3(b) indicates that the OM-OFDM method with a $\overline{\Upsilon} = -7$ dB and $\overline{\Upsilon} = 3$ dB offers better detection characteristics than an OFDM transmission. Similarly, for a Rayleigh fading channel, depicted in Fig. 7.4(a) and Fig. 7.4(b), for a $\overline{\Upsilon} = -7$ dB and

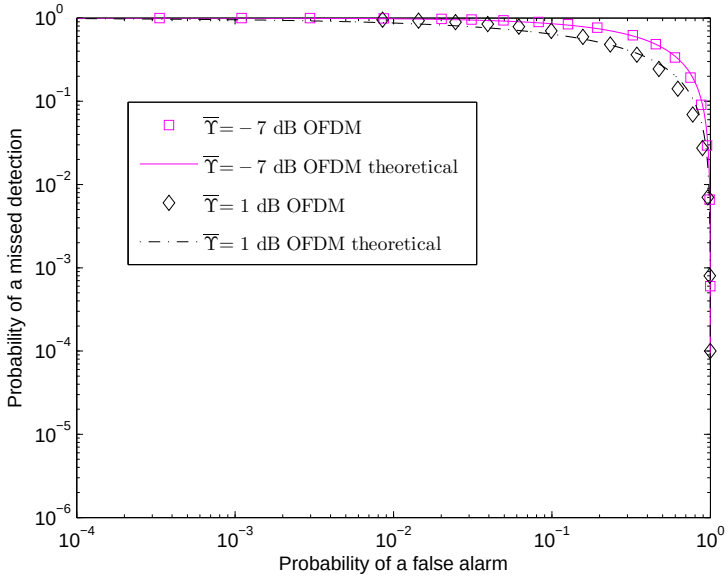

(a) A 12 dB PAPR OFDM transmission

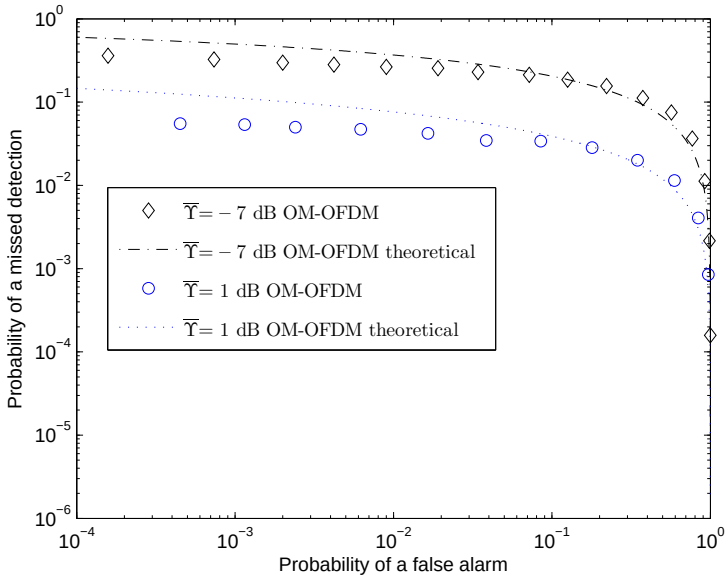

(b) OM-OFDM transmission

Figure 7.4: A ROC comparison between a theoretically predicted (Eq (7.16)) and simulated OFDM and OM-OFDM transmission through a Rayleigh fading channel.

$\overline{\Upsilon} = 1$ dB, OM-OFDM offers better detection characteristics than an OFDM transmission. In the next section a more comprehensive comparison is provided.

7.5 RESULTS AND DISCUSSION

In this section, by using the 2k mode of the DVB-T2 standard, 16-QAM Gray-coded OFDM and OM-OFDM data were transmitted through a Rician, (K=5dB), Rayleigh and a 3-tap typical-urban frequency selective fading channel. The pilot symbol placement for both OM-OFDM and OFDM, can be found in the DVB-T2 standard. Similarly, the 3-tap typical-urban area model was obtained from Patzold [96]. Identical throughputs were used to ensure a fair comparison between the various methods and perfect carrier and timing synchronisation was assumed. Both methods conform to the spectrum mask and throughput requirements imposed by the DVB-T2 standard. This OFDM type of transmissions would typically be encountered in the development of the IEEE 802.22 standard in the spectrum sharing of the TV band. For a Rician channel, depicted in Fig. 7.5, the P_{md} of an OM-OFDM ($\overline{\Upsilon}$=−7 dB)

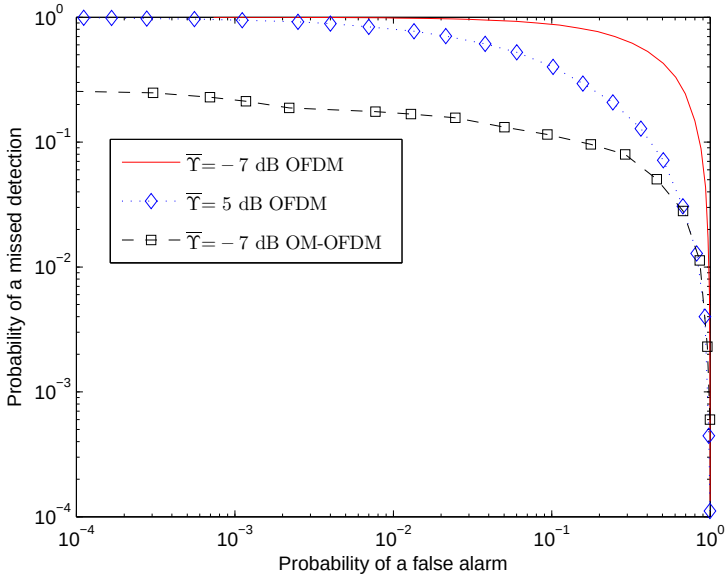

Figure 7.5: ROC comparison over a Rician fading (K=5dB) channel.

transmission is 9.6×10^{-2} and the P_{md} for both OFDM ($\overline{\Upsilon}$=−7 dB and $\overline{\Upsilon}$=5 dB) transmissions are 0.86 and 0.4 (at a $P_{fa} = 10^{-1}$), respectively. Similarly for a Rayleigh channel, depicted in Fig. 7.6, the P_{md} of an OM-OFDM transmission is 1.8×10^{-1} and the P_{md} for both OFDM ($\overline{\Upsilon}$=−7 dB and $\overline{\Upsilon}$=5 dB) transmissions are 0.84 and 0.4 (at a $P_{fa} = 10^{-1}$), respectively. In addition, for a 3-tap typical urban frequency selective fading channel, depicted in Fig. 7.7, the P_{md} of an OM-OFDM transmission is 1×10^{-1} and the P_{md} of both OFDM

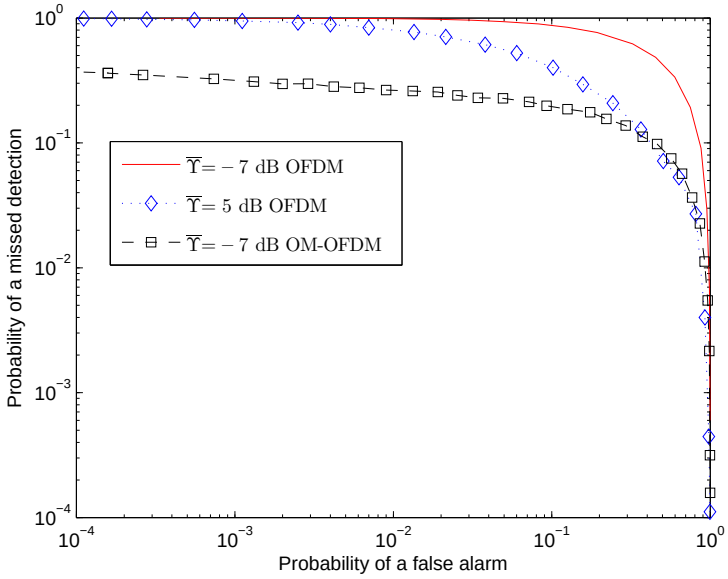

Figure 7.6: ROC comparison over a Rayleigh fading channel.

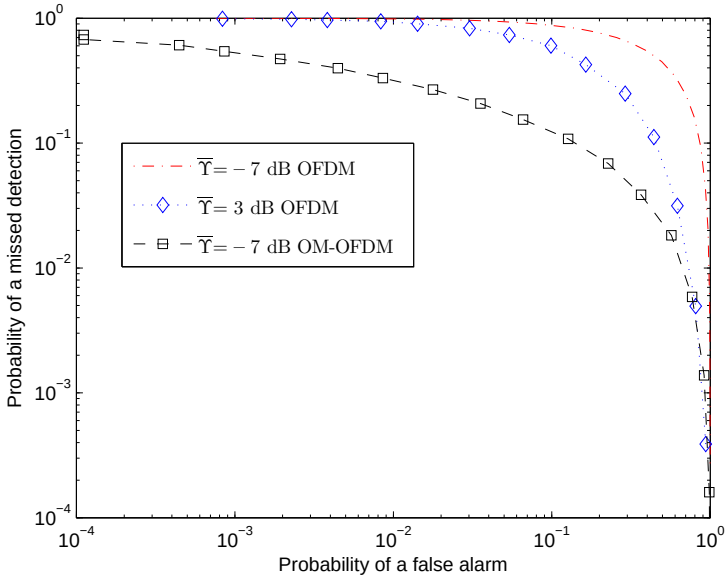

Figure 7.7: ROC comparison over a 3-tap typical urban area.

($\overline{\Upsilon}$=−7 dB and $\overline{\Upsilon}$=5 dB) transmissions are 0.9 and 0.53 (at a $P_{fa} = 10^{-1}$), respectively. All three comparisons, depicted in Fig. 7.5, Fig. 7.6 and Fig. 7.7 have been summarised in Table 7.2 and Table 7.3. From Table 7.2, the P_{md} of an OM-OFDM transmission is between $0.096 - 0.18$ and the P_{md} of an OFDM transmission is between $0.84 - 0.9$ (at a $P_{fa} = 10^{-1}$ and average SNR of -7dB) for a Rician, Rayleigh and frequency selective fading channel

Table 7.2: Summarised P_{md} results for a $\overline{\Upsilon}$=−7 dB OFDM and $\overline{\Upsilon}$=−7 dB OM-OFDM transmission at a $P_{fa} = 10^{-1}$

Channel	P_{md}	
	OFDM	OM-OFDM
Rician	0.86	0.096
Rayleigh	0.84	0.18
FSF	0.9	0.1

Table 7.3: Summarised P_{md} results for an OFDM and OM-OFDM transmission at a $P_{fa} = 10^{-1}$

Channel	P_{md}				
	$\overline{\Upsilon}$ (dB)	OFDM	$\overline{\Upsilon}_o$ (dB)	OM-OFDM	$\overline{\Upsilon} - \overline{\Upsilon}_o$ (dB)
Rician	5	0.4	−7	0.096	12
Rayleigh	5	0.4	−7	0.18	12
FSF	3	0.533	−7	0.1	10

conditions. This indicates that an OM-OFDM transmission offers significantly better detection characteristics than an OFDM transmission. Similarly in Table 7.3, the P_{md} of an OM-OFDM transmission is shown to be between $0.096 - 0.18$ and the P_{md} of an OFDM transmission is between $0.4 - 0.53$ (at a $P_{fa} = 10^{-1}$) for varied channel conditions. In addition, in Table 7.3, the OM-OFDM method is shown to operate at a 10 dB - 12 dB lower SNR value than an OFDM transmission, while still offering better detection characteristics than an OFDM transmission under various channel conditions. The significant performance improvement offered by OM-OFDM is possible (as discussed Section 7.3) because of the presence of a dominant frequency component in an OM-OFDM transmission.

7.6 CONCLUSIONS

The OM-OFDM method has been proposed for cognitive radio applications. An examination of an OM-OFDM bandwidth occupancy highlights its attractive detection properties. Furthermore, a simplified theoretical closed-form relationship between the probability

of a missed detection and the probability of a false alarm, for an unknown deterministic signal, is derived and validated. Previous expressions have been derived which relate the probability of a missed detection to the probability of a false alarm. However, they have not been presented in such a closed-form expression which can be used for any unknown deterministic signal (for instance OFDM and OM-OFDM).

Thereafter, by using energy detection, the offset modulation method is shown to operate at a 10 dB - 12 dB lower SNR value than an OFDM transmission, while still offering better detection characteristics than an OFDM transmission under Rician, Rayleigh and frequency selective fading conditions. The ROC curves indicate that the P_{md} of an OM-OFDM transmission is between $0.096 - 0.18$ and the P_{md} of an OFDM transmission is between $0.84 - 0.9$ (at a $P_{fa} = 10^{-1}$ and average SNR of -7dB) for Rician, Rayleigh and frequency selective fading channel conditions. These aspects make it a promising candidate for cognitive radio.